Computational Materials Science 172 (2020) 109347

Contents lists available at ScienceDirect

Computational Materials Science

journal homepage: www.elsevier.com/locate/commatsci

Unraveling the non-monotonic ageing of metallic glasses in the metastability-temperature space

Chaoyi Liu[a], Xin Yan[b,c], Pradeep Sharma[c,d,e], Yue Fan[a,*]

[a] Department of Mechanical Engineering, University of Michigan, Ann Arbor, United States
[b] School of Mechanical Engineering and Automation, Beihang University, Beijing, China
[c] Department of Mechanical Engineering, University of Houston, United States
[d] Department of Physics, University of Houston, United States
[e] Material Science and Engineering Program, University of Houston, United States

ARTICLE INFO

Keywords:
Metallic glasses
Computational modeling
Energy landscape theory
Ageing phenomenon

ABSTRACT

Ageing behaviors of metallic glasses are investigated by atomistic modeling in a broad range of processing histories and thermal conditions. By employing an enhanced data-mining analysis, a non-monotonic ageing phenomenon is resolved with high precision. It is observed that there exists a non-linear correlation between the system's metastability and the critical temperature where maximum ageing rate occurs. In further conjunction with the recently developed energy landscape theory to circumvent the time-scale limitations of molecular dynamics, the ageing rate contours over ten orders of magnitude are mapped out in the metastability-temperature space. Such map enables a natural explanation to the experimentally observed shift of exothermic signal, which cannot be provided by existing models. Implications of the present study for understanding the mechanical properties of amorphous alloys are also discussed.

1. Introduction:

The disordered nature of atomic packing, metastability and other related aspects endow metallic glasses with several unique features that suggest applications in high strength materials [1–3], for wear and corrosion protection [4,5], radiation resistance [6], catalysis [7], magnetism [8], and electronics [9,10]. As inherently non-equilibrium systems, metallic glasses exhibit physical ageing, which critically depends on the processing histories [11–15] and in turn impacts the system's emergent properties. Moreover, the thermal and mechanical behaviors of metallic glasses are often coupled with each other, and experiments show that a sample with more pronounced exothermic signal during thermal scanning may have better ductility [16]. Unfortunately, a fundamental knowledge pertaining to the relaxation processes in metallic glasses, *i.e.* their ageing/rejuvenating behavior and interplay with surrounding environment, still remains elusive. For example, Slipenyuk and Eckert have noted [17] that the significant shift of exothermic peaks in their differential scanning calorimetry (DSC) experiments cannot be correctly captured by existing models.

In the present study, we employ atomistic simulations to study the annealing behavior of metallic glasses at various temperatures and thermal processing histories. By utilizing an enhanced data-mining statistical algorithm, we are able to construct a high-resolution pixel map of the relaxation behavior for various environments. Significantly, we can resolve the clear phenomenon of non-monotonic ageing, and the temperature corresponding to the maximum ageing rate shows a non-linear dependence on the system's processing history (*i.e.* relaxation level). We demonstrate that the complex ageing behavior can be quantitatively attributed to the energy imbalance along with the elementary hopping processes in the potential energy landscape (PEL). In further conjunction with the recently developed PEL-based rate theory [18], we are able to map out the system's ageing rate contour lines across multiple orders of magnitude and naturally explain the shift of exothermic peaks mentioned above. More specifically, the nature of broad activation energy (E_A) spectrum in disordered solids would result in a T-dependent average $< E_A >$. At low temperature $< E_A >$ becomes smaller, which leads to a boosted ageing behavior and consequently a noticeable exothermic behavior as observed in experiments. Without invoking free fitting parameters, the present study thus enables a mechanistic and predictive understanding towards the non-equilibrium evolution in amorphous solids.

* Corresponding author.
E-mail address: fanyue@umich.edu (Y. Fan).

https://doi.org/10.1016/j.commatsci.2019.109347
Received 17 September 2019; Received in revised form 8 October 2019; Accepted 11 October 2019
0927-0256/ © 2019 Elsevier B.V. All rights reserved.

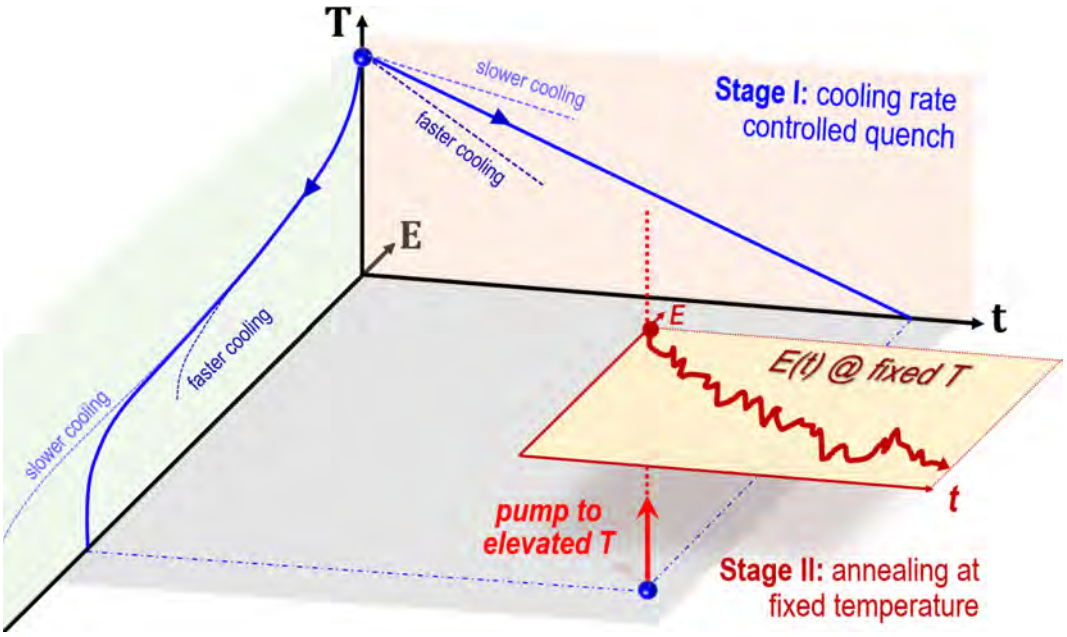

Fig. 1. Thermal protocols of MD simulations. System is firstly equilibrated at 2000 K and then annealed to 0 K with different cooling rates. Samples at different IS energy states are then annealed under isothermal condition with different temperatures, and the energy variation curves during the annealing processes are monitored.

2. Materials and methods

To examine the annealing behaviors of metallic glasses at various conditions, we follow a two-stage protocol in MD simulations illustrated in Fig. 1. First, the high-temperature equilibrated metallic liquid ($Zr_{44}Cu_{56}$) is quenched to 0 K at a controlled cooling rate (ranging from 0.01 K/ps to 10 K/ps); then in the second stage, the sample is pumped to and held at an elevated temperature (ranging from 500 K to 850 K) for 10 ns, during which the energy variation is monitored. By tuning the cooling rates in stage I, and the temperatures in stage II, we can investigate the system's annealing behavior at various initial stability and thermal conditions. It is known that the properties of disordered materials are largely controlled by their inherent structures (IS) [19–21], *i.e.* the local minima in the PEL. Therefore, instead of focusing on the total energy of the system, in stage II we only focus on the variation of IS energy by removing the kinetic energy. To be more specific, during MD annealing simulations the system's instantaneous configurations are recorded every 50 ps. The IS are then obtained by minimizing those configurations to local minima in the PEL, and the corresponding potential energy are the E_{IS} to be monitored in this study. More details can be found in Appendix A1.

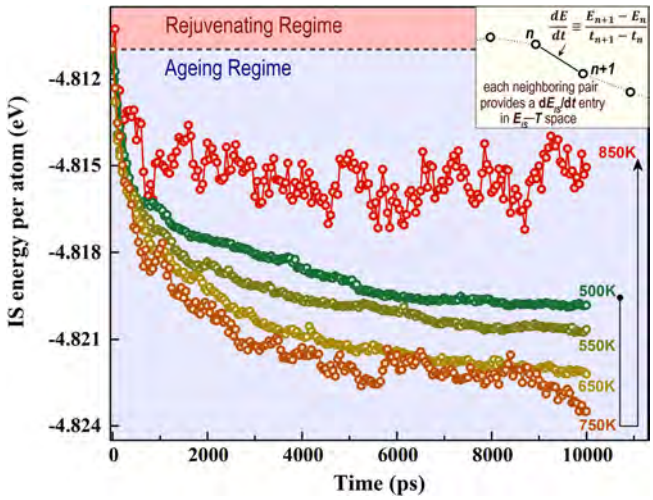

Fig. 2. IS energy variation curves of a sample constructed from 10 K/ps cooling rate. This sample was annealed in the 500–850 K temperature range, and an apparent non-monotic behavior is observed. Inset: schematic illustration of statistical treatment to acquire energy evolution rate from annealing curves.

3. Results

3.1. Non-monotonic ageing phenomenon.

Following the aforementioned protocol, in Fig. 2 we show the IS energy variation curves at different temperatures for a sample that was prepared at the 10 K/ps cooling rate. All the curves collapse in the beginning because, at $t = 0$, the relaxation has not started yet. As can be seen, the IS energy continuously decreases for all these conditions, suggesting that the sample undergoes an ageing behavior in the investigated temperature regime. On the other hand, the ageing rate evidently shows a *non-monotonic* dependence on the temperature. For example, in the regime from 500 K to 750 K by increasing the temperature, the IS energy drops to a deeper level within the same amount of time, suggesting a larger ageing rate; while by further increasing the temperature to 850 K, the annealing curve becomes much flatter and the overall ageing rate obviously becomes smaller. Therefore, there must exist a critical temperature, where the ageing rate reaches its maximum. In Fig. 2 we only show the results of one sample to avoid the plot being overcrowded. We remark that all other samples qualitatively exhibit a similar annealing behavior although as will be discussed below, the quantitative maximum ageing rate temperature varies in different samples in a complex manner.

To better understand annealing behavior described in the preceding paragraph, it is critical to quantify the ageing rate for various environments. It is clear from Fig. 2 that the ageing rate of the system is highly non-linear and very sensitive to both the IS energy level and the temperature. Therefore, to precisely quantify the ageing rate we should, in principle, prepare a large number of samples at different IS energy states and anneal them at many different temperatures. This would, however, be computationally too expensive. Here, we introduce an

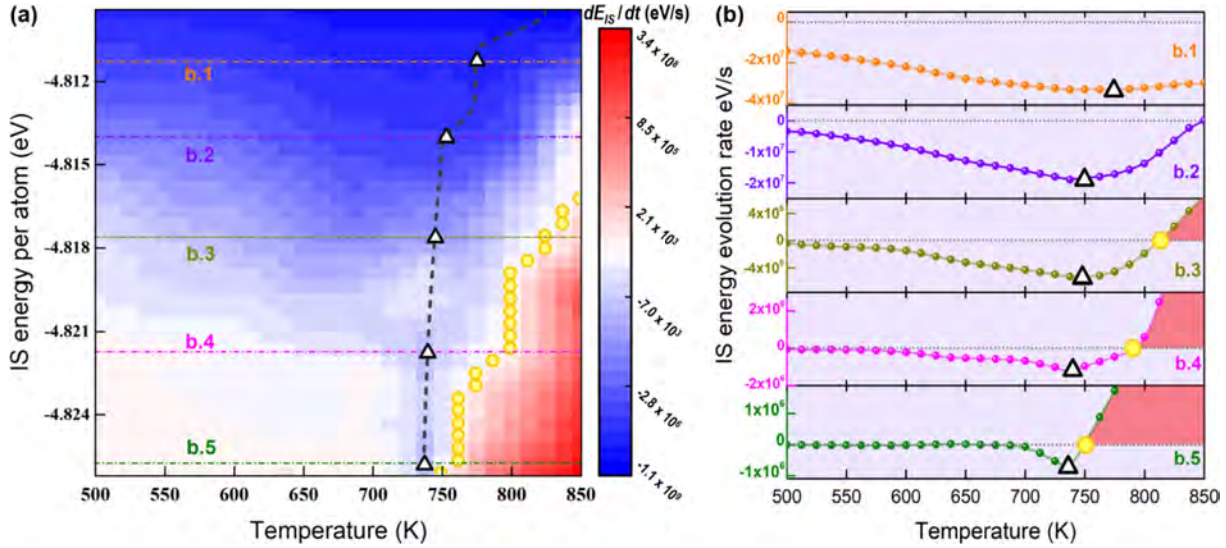

Fig. 3. (a) Pixel map of energy variation rate in E_{IS}—temperature space. Blue and red regimes correspond to ageing and rejuventaing behaviors, respectively. The black dash line denotes the critical temperatures where system reaches the maximum ageing rate at a certain energy level; while the open yellow circles are the retrieved steady state, where $dE_{IS}/dT = 0$. (b) IS energy variation rates along 5 horizontal scans at different energy levels denoted in (a). Positions of maximum ageing rate and ageing/rejuvenating transition are marked by the triangles and circles, respectively.

enhanced statistical treatment illustrated in the inset of Fig. 2, which enables a more efficient data mining process. To be more specific, we calculate the slopes of neighboring data points in each individual $E(t,T)$ annealing curve. For example, the slope between the n th and $n+1$ th points can be calculated as $(E_{n+1} - E_n)/(t_{n+1} - t_n)$, and this is essentially the ageing rate dE_{IS}/dt at the prescribed temperature T and IS energy level $(E_{n+1} + E_n)/2$. Following such an algorithm, each neighboring pair would provide an effective entry of ageing rate in the E_{IS}—T space, and by considering all the neighboring pairs for all the annealing curves, the statistics are significantly enhanced. While in the raw data only a series of discrete temperatures are considered, such enhanced statistics allows us to map the scattered entries into a quasi-continuum contour plot by using the thin-plate spline (TPS) interpolation method. More details may be found in Appendix. A2.

The obtained pixel map of the ageing rate, dE_{IS}/dt, is shown in Fig. 3(a), where each pixel is colored according to the log-scaled magnitude of the ageing rate. In the blue regime, dE_{IS}/dt is negative and the system undergoes a normal ageing behavior; while in the red regime, dE_{IS}/dt becomes positive and the system, in fact, undergoes a rejuvenating behavior. The transition boundary between the two regimes, in other words where the system stays in steady-state $dE_{IS}/dt = 0$, is marked by the open yellow circles. Another important observation is that, a non-monotonic ageing behavior can be clearly resolved in the pixel map. In other words, if we gradually increase the temperature while keeping the IS energy level fixed, then the ageing rate will firstly increase and then decrease, reaching a maximum value prior to the ageing/rejuvenating transition temperature. Fig. 3(b) shows the results along 5 such horizontal scans at different energy levels indicated in Fig. 3(a), and the positions of maximum ageing rates are marked by open black triangles. It can be seen that, as IS energy decreases, the maximum ageing rate temperature shifts towards the left side and meanwhile its interval with the ageing/rejuvenating transition temperature becomes narrower.

3.2. Ageing rate contours & exothermic peak shift.

To unravel the reason for why the maximum ageing rate temperature is shifting, here we seek the recently developed PEL model [18], which has successfully explained the ageing/rejuvenating crossover in disordered solids. From the PEL perspective [19–22], the evolution of disordered materials consists of a series of elementary hopping processes between different IS. As illustrated in Fig. 4(a), an individual hopping can be decoupled into two stages: the up-hill activation stage from the present IS to the connecting saddle states with the activation barrier E_A and the down-hill relaxation stage from the saddle states to the next IS with the energy relaxation E_R. Assuming at moment t the system occupies a certain IS with the energy of $E_{IS}(t)$, then at the next moment $t + \Delta t$ after hopping, the energy change is given by $(E_A - E_R)$. A consequent differential equation for E_{IS} evolution can then write as [18]:

$$\left\langle \frac{dE_{IS}(t)}{dt} \right\rangle \approx \frac{\langle E_{IS}(t+\Delta t) - E_{IS}(t)\rangle}{\langle \Delta t\rangle} = \nu\cdot\exp\left(-\frac{\langle E_A\rangle}{k_B T}\right)\cdot\langle E_A - E_R\rangle \tag{1}$$

where $\langle \Delta t\rangle = [\nu\cdot\exp(-\langle E_A\rangle/k_B T)]^{-1}$ represents the average residence time in the current IS, $\nu$is the jump frequency which includes the entropy effect [18] and $k_B T$ has its usual meaning. Note that $\langle\cdots\rangle$ represents the average over all possible hopping paths, because there exist multiple transition pathways in the PEL of amorphous materials and they should all be taken into consideration. In other words, E_A and E_R no longer have explicit values as in the crystalline counterparts. Instead, they are expected to be described by the E_{IS}-dependent broad spectra [23–25], $P(E_A\,|E_{IS})$, and $P(E_R\,|E_{IS})$, respectively. And their average values should be calculated as:

$$\langle E_A(E_{IS}, T)\rangle = -k_B T\cdot\ln\left[\int P(E_A\,|E_{IS})e^{-\frac{E_A}{k_B T}}dE_A\right],$$
$$\langle E_R(E_{IS})\rangle = \int E_R\cdot P(E_R\,|E_{IS})\cdot dE_R\,. \tag{2}$$

Note that the up-hill activation stage is essentially a thermal process, and the Boltzmann weighting factor has to be incorporated in the averaging calculation. As a result, the average activation barrier $\langle E_A\rangle$ in general becomes a function of both E_{IS} and T. In contrast, the relaxation stage is a spontaneous downhill process, which does not need the thermal assistance [26]. Therefore, no Boltzmann factor is involved in the relaxation stage, and the expected relaxation energy $\langle E_R\rangle$ is only a function of E_{IS}, as expressed in Eq. (2). It is also worth noting that, the validity of Eqs. (1 and 2) requires that $P(E_A\,|E_{IS})$ and $P(E_R\,|E_{IS})$ are independent from each other. While it is very difficult to prove such assumption analytically, the systematic PEL samplings both in metallic glasses [18] and in amorphous Si [27] have shown strong evidence on the independence of E_A- and E_R-distributions. We therefore assume such approximation is effective in the present study.

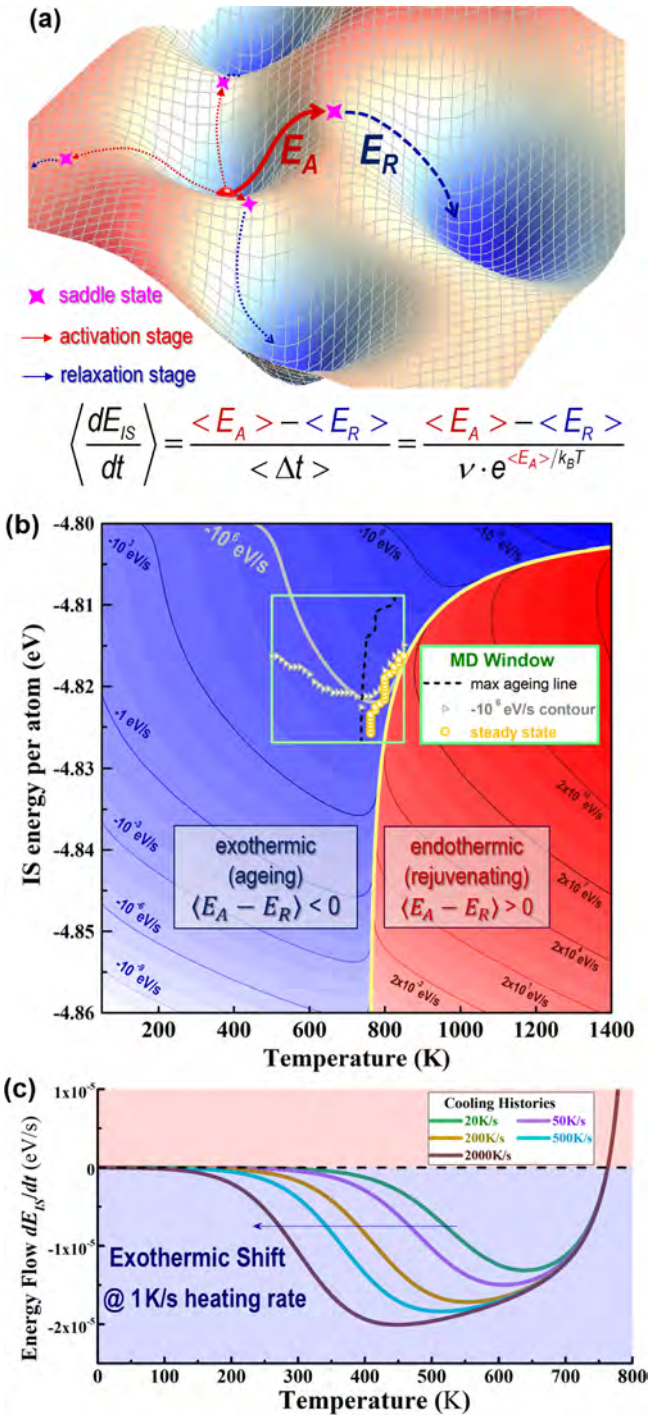

Fig. 4. (a) Schematic illustration of IS energy variation during elementary hooping on PEL. The IS energy change is induced by the imbalance of activation energy E_A and relaxation energy E_R.The distributions of E_A and $E_R$at different energy levels can be directly probed by atomistic sampling technique. In the present study we utilize the recently obtained spectra in the same system [18]. (b) Theoretically calculated results of intrinsic energy variation rate by Eq. (1), in the E_{IS}—T space. Key features of MD simulation, including the maximum ageing rate position (black dashed curve), the ageing/rejuvenating transition boundary (open yellow circle), and the position of constant ageing rate at -10^6 eV/s (grey triangle), are also presented for comparison. (c) Prediction of PEL model on the exothermic behavior at realistic conditions. The samples are first prepared at the cooling rate from 20 K/s to 2000 K/s, by solving Eq. (1) with a time-dependent T control. Then those samples are subject to a following heating treatment, again by varying the T in Eq. (1) at 1 K/s. These represent similar conditions to experiments [17] and far beyond MD's accessibility. For a less annealed sample (*i.e.* higher cooling rate), the exothermic signal clearly shifts towards the low temperature region, which is very well consistent with the real measurement.

Once the probability distribution functions of $P(E_A|E_{IS})$ and $P(E_R|E_{IS})$ are available, one can readily calculate the $\langle E_A \rangle$ and $\langle E_R \rangle$ through Eq. (2), and further quantify the dE_{IS}/dt at prescribed (E_{IS},T) condition through Eq. (1). Recent advances in PEL-sampling techniques [27–29] have made it possible to directly probe the high-fidelity E_A and E_R spectra in disordered materials. In the present work recently obtained $P(E_A|E_{IS})$ and $P(E_R|E_{IS})$ in the same system [18] are utilized in Eq. (2), for the sake of benchmarking the results in Fig. 3(a) and meanwhile saving some computational costs.

Fig. 4(b) shows the calculated results of dE_{IS}/dt by Eq. (1) in the broad E_{IS}—T space. Overall the entire map is divided into two regimes: in the blue side there is $\langle E_A - E_R \rangle < 0$, and the system undergoes an ageing (exothermic) process; while in the red side there is $\langle E_A - E_R \rangle > 0$, and the system undergoes a rejuvenating (endothermic) process. The underlying physics for such sign flip is straightforward: as discussed above, due to the broad distribution and incorporated Boltzmann factor, $\langle E_A \rangle$becomes T-dependent and according to Eq.(2), $\langle E_A \rangle$ is a monotonically increasing function of T; while on the other hand, $\langle E_R \rangle$is T-insensitive. Therefore, by gradually increasing the temperature, one naturally expects the value of $\langle E_A - E_R \rangle$ to change from negative to positive.

As aforementioned, such ageing/rejuvenating crossover has been reported earlier [18] and in the present study we will restrict our attention to the origin of complex ageing in the blue regime, which has not been elucidated before. As seen by the contour lines in Fig. 4(b), a clear non-monotonic ageing phenomenon can be resolved. In other words, by increasing the temperature in the blue regime, the ageing rate increases first, reaching its maximum value at some intermediate stage, and then will start to decrease until zero at the ageing/rejuvenating transition point. Such non-monotonic behavior can be naturally explained by the PEL model: as reflected in Eq. (1), the IS energy variation rate is determined by two key factors, $\langle E_A - E_R \rangle$, and $\exp(-\langle E_A \rangle / k_B T)$, respectively. The first factor has been discussed above, that the sign of $\langle E_A - E_R \rangle$ is negative in the blue regime and its absolute value decreases as a function of T. As for the second factor, it can be analytically proved that its value becomes larger monotonically as T increases. As a result, the opposite dependences on T yield the non-monotonic ageing behaviors.

The mechanism map so-constructed covers a wide span of E_{IS} , T, and relaxation timescales—well beyond the capabilities of MD. The reason why such calculation is not limited by the short timescales inherent in conventional MD is because in Eq. (2) the entire activation energy spectrum $P(E_A|E_{IS})$ is considered, which naturally includes the high-barrier processes and thus slow kinetics. To verify such map, we first examine its results in the space window where MD is known to be valid. To be more specific, some key results of MD simulations retrieved from Fig. 3(a) are also presented in the green box of Fig. 4(b). It can be seen that the maximum ageing rate position (black dashed curve) indeed closely aligns with the minima of the contour lines. The ageing/rejuvenating transition boundary (open yellow circle) and the position of constant ageing rate at -10^6 eV/s (grey triangle) are also reasonably consistent with the independent PEL calculations through Eqs. (1 and 2).

Another important point we would like to note is that, the wide span of orders of magnitude in the contour line values in Fig. 4(b) makes it possible to directly compare with experiments. As discussed in the beginning of this paper, Slipenyuk and Eckert measured the exothermic signals of metallic glasses samples with different thermal processing histories and observed a significant shift of exothermic peaks that cannot be correctly explained by existing models [17]. In their experiments, the samples were prepared with a centrifugal casting technique, implying that the cooling rates ought to be in the order of $10^2 \sim 10^3$ K/s [30]. The following DSC scan was controlled at ~1 K/s heating rate. Fig. 4(c) shows the calculated energy flow curves by Eq. (1) during the heat scan at similar conditions (details of the numerical integration can be found in Appendix. A3.) A clear shift of exothermic

signals is naturally resolved, showing a good agreement with the DSC measurement [17].

4. Discussion

We believe the significant shift of exothermic peaks in Fig. 4(c) can be attributed to the nature of broad E_A spectra in disordered materials. To be more specific, according to Eq. (2) the broad spectra $P(E_A|E_{IS})$ result in a T-dependent $\langle E_A\rangle$. At lower temperature $\langle E_A\rangle$ becomes smaller, and the kinetics factor in Eq. (1), namely $\exp(-\langle E_A\rangle/k_BT)$, will be boosted, leading to a noticeable exothermic behavior as observed in experiments. On the contrary, in most existing models (*e.g.* free volume theory [31,32], shear transformation zone model [33], *etc*) the activation energy is usually assigned with a constant fitting number, which would severely suppress the kinetics at low T in an exponential manner. This is why the existing models can only explain the different strength of the exothermic peaks [17], but not their shift along the T-axis as observed in experiments. In fact, Slipenyuk and Eckert suggested that, to explain their measurements, there should exist a continuously distributed activation barriers [17], and our present results provide fundamental support to such hypothesis. Note that a fully quantitative comparison between the present calculations and their experiments would be challenging, due to the difficulty of identifying the precise cooling rate in experiment and the more complex chemical composition in real samples. Nonetheless, without invoking free parameters, the clear shift captured in Fig. 4(c) is remarkable and encouraging, because it reveals that the nature of complex annealing behavior originates from the underlying PEL structures.

Admittedly, as seen in Fig. 4(b), MD results and PEL predictions do not perfectly align with each other. We attribute such discrepancies to the following two reasons: (i) Eq. (1) in PEL model is essentially a mean-field theory that averages out all possible elementary hopping events, and the calculated contour lines are therefore continuous and smooth. However, fluctuations are inevitable in MD simulations and the results are thus more scattered; (ii) In the data-mining process, the energy variation rates are calculated through the linear slope between two adjacent points in the anneal curve illustrated in Fig. 2. Although the 50 ps interval selected in the present study is relatively small comparing with intrinsic relaxation timescale in glasses, the ageing rate after all is still non-linear, which presumably leads to some errors in the estimated results and gives rise to the deviations from PEL calculation.

In spite of these (relatively minor) discrepancies, we remark that almost no empirical assumptions (in a relative sense) or free parameters were invoked in the PEL model. While the EAM potential employed in the present study was developed based upon *ab initio* calculations [34], it is in principle still empirical. We would like to note, however, the spectra of $P(E_A|E_{IS})$ and $P(E_R|E_{IS})$ are directly probed by atomistic sampling technique [18] in a "bottom-up" manner, rather than being numerically fitted to experiment. From such sense the present model is relatively more fundamental or less empirical with respect to the existing methods. Given this, the extent of the agreement in Fig. 4(b) is indeed remarkable. In addition, with its capabilities in accessing to realistic timescales and capturing experimental phenomena as reflected in Fig. 4(c), we see a considerable potential of the PEL model for understanding and predicting the complex phenomena in disordered non-equilibrium materials. Very interestingly, and importantly, Cao *et al*'s recent study [35] shows that a PEL-centric modeling framework can also elucidate the nature of the qualitatively different rheological behaviors of glassy materials under mechanical loading, which was attributed to the interplay between thermal and stress activations during the barrier-hopping processes on the fractal PEL.

It is worth noting that, while the main scope in the present study has been focused on the non-monotonic ageing and exothermic behavior of metallic glasses, we believe it could also provide deep insights into some other important aspects, such as the STZs and β relaxations. To be more specific, experiments show that a more pronounced exothermic signal corresponds to a better ductility [16], and usually an enhanced ductility suggests a larger number density of STZs or flow units in the sample [36]. In the present work, the origin of a stronger exothermic signal can be attributed to a higher intrinsic ageing rate, and according to the contour lines in Fig. 4(b), higher intrinsic ageing rate would happen at higher E_{IS} level. Therefore, it seems to suggest that a sample at higher energy state would contain a larger population of STZs, which qualitatively is not so surprising. By taking a further step, the intrinsic ageing rate is ultimately determined by the energy imbalance during the IS hopping in the PEL. Recent study [37] shows that at higher energy level the IS are more crowdedly distributed, and a remarkable similarity to the STZ theory has been observed. Therefore, there is indeed deep connections between the two models. We believe a similar spirit would also hold for β relaxations processes, which are known as elementary hopping between neighboring IS in the PEL [19,21,38,39]. Because following the above-mentioned logic, at higher energy level there are more crowdedly distributed IS and thus one should expect a pronounced β relaxation and consequently, a better ductility. This is in excellent agreement with existing studies [36,40–43], which have demonstrated that a pronounced β relaxation indicates a more frequent collective atomic jumps and would lead to a stronger exothermic signal and an enhanced ductility of the sample.

As a final note, shear band formation is known as the roadblock of preventing the wide application of metallic glasses. A popular shear banding mechanism is the four-zone hierarchy structure of shear embryo embedded in a temperature gradient proposed by Shimizu *et al.* [26]. Such embryonic structure is named ARGL, representing aged glass, rejuvenated glass, glue, and liquid zones, respectively, from high to low temperatures. Therefore, the capability of accurately calculating the ageing/rejuvenating contour lines over a broad temperature range shown in Fig. 4(b) can provide fundamental basis to the ARGL model and thus shed light on the understanding of heterogenous deformation in metallic glasses.

5. Conclusion

In conclusion, by employing an enhanced statistical analysis to mine the data generated by atomistic modeling at various conditions, we are able to resolve the non-monotonic and non-linear ageing behavior of metallic glasses with high precision. It is demonstrated that such complex ageing phenomenon can be satisfactorily explained by the energy imbalance along with the non-equilibrium evolution in the PEL. Significantly, the PEL model is not limited by the short timescales inherent in conventional MD because the entire activation energy spectrum is entailed in the PEL, which naturally includes the high-barrier processes and thus slow kinetics. We further demonstrated that the broad activation energy spectrum would result in a temperature-dependent $\langle E_A\rangle$ and naturally lead to a significant shift of exothermic signals at experimental conditions, which cannot be explained by existing methods where the activation energy is usually set as a fitted constant number. The fitting-free feature of this model, as well as its accessibility to experimental timescales, makes the present study not only can unravel the mystery of ageing in metallic glasses but could also be broadly applicable to many other important non-equilibrium systems containing strong disorder, such as interfaces, gels, and polymers.

6. Data availability statement

The datasets generated and analyzed during the current study are available from the corresponding author upon reasonable request.

CRediT authorship contribution statement

Chaoyi Liu: Data curation, Formal analysis, Investigation, Methodology, Software, Validation, Visualization, Writing - original draft, Writing - review & editing. **Xin Yan:** Data curation, Formal

analysis, Investigation, Software, Validation, Visualization, Writing - original draft, Writing - review & editing. **Pradeep Sharma:** Formal analysis, Investigation, Resources, Validation, Writing - original draft, Writing - review & editing. **Yue Fan:** Conceptualization, Formal analysis, Funding acquisition, Investigation, Methodology, Project administration, Resources, Supervision, Validation, Writing - original draft, Writing - review & editing.

Declaration of Competing Interest

The authors declare that they have no known competing financial interests or personal relationships that could have appeared to influence the work reported in this paper.

Acknowledgement

This work is supported by the U. S. Army Research Office under Grant No. W911NF-18-1-0119. P. S. would like to acknowledge the M. D. Anderson Professorship.

Appendix

A1: A well-known metallic glass former $Zr_{44}Cu_{56}$ consisting of 2000 atoms is adopted in our MD simulations and such selection was based on the following considerations: (i) there exists a robust and realistic embedded-method (EAM) potential [34] for such model and it has been widely used by the community [44–50]; (ii) the high-fidelity spectra of $P(E_A|E_{IS})$ and $P(E_R|E_{IS})$ in such model are available [18], which could then ease the benchmark of the results in Fig. 3(a) and meanwhile save some computational costs. The MD annealing study follows a two-stage protocol. At the first stage, the system is firstly equilibrated at 2000 K ($\sim 3T_g$) for 1 ns with the time step of 1 fs and then quenched to 0 K within 4 orders of magnitude change in cooling rates, from $0.01K/ps$ to $10K/ps$. At the second stage, samples at different energy levels are pumped to and held at an elevated temperature for 10 ns, in the range of 500 K ~ 850 K. During such annealing process, the snapshot configurations are dumped every 50 ps. The IS of these dumped configurations are then acquired by a steepest descent minimization algorithm built in LAMMPS. In addition, each condition is simulated for 5 times to reduce data fluctuation.

Note that commonly employed simulation sizes for glassy materials span from a few hundred [20,51], to a few thousand [27,29,52], and dozens of thousands [53,54]. No significant size effects have been observed in terms of the IS energy [55], which is the central focus of the present study. Therefore, the selection of 2000 atoms is based on the balance of reliability and calculation efficiency. To further confirm that the size effect does not play a critical role in our present study, we also conducted the simulation in a larger-size system containing 4000 atoms. As can be seen in Fig. 5, no statistical differences can be observed. We therefore believe the 2000-atoms system can reflect the correct physics and the obtained results in the main text are reliable.

A2: In the inset of Fig. 2 in the main text we showed how to use statistics method to extract energy evolution rate at certain temperature and IS energy level from isothermal annealing data. Such treatment can provide large amount of discrete data entries of dE_{IS}/dt, and these raw data points are shown below in Fig. A1. It is noted that, although discretely distributed, the aging and rejuvenating regimes are clear. These results are further converted into a pixel plot (Fig. 3a in the main text) by employing the thin-plate spline (TPS) interpolation algorithm [56]. To be more specific, the averaged values are firstly chosen for overlapped points in Fig. A1. Then a 2D surface in the T—E_{IS} space is constructed by minimizing the sum of square of differences between a fit function and these data points. With the fitted 2D function, a continuous pixel map can thus be obtained. The TPS interpolation process is implemented using OriginLab, and the smoothing parameter is set as 6 in the present study.

As discussed above, the pixel map (Fig. 3a in the main text) is obtained by mining the data of 10 ns MD simulations. One can certainly do longer MD simulations with nowadays computational power, but we would like to note that the effective data-mining algorithm used in the present study allows to obtain the high-resolution results without the necessity of doing long time MD simulations. For example, the similar spirit has been shown before in Deng and Schuh's work in a grain boundary system [57], where they demonstrated that with enhanced statistical algorithm to better utilize the raw MD data, even within only a few hundred pico-seconds, the precision of the calculations can be tremendously improved and reliable results can be obtained.

To confirm that the key is the effective data mining rather than the length of MD simulation time, we have performed a longer MD simulation up to 30 ns in the same system. As seen in Fig. A2, there are no discernable changes to the non-monotonic ageing phenomena.

A3: The exothermic behaviors in Fig. 4(c) are calculated by numerically solving Eq. (1) with T as a controlling parameter. To be more specific,

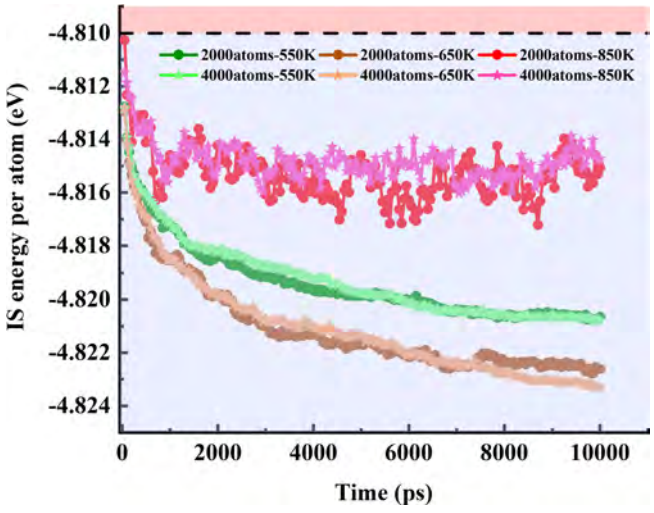

Fig. 5. Aging behaviors in metallic glass modeling system with different sizes. No significant differences are observed.

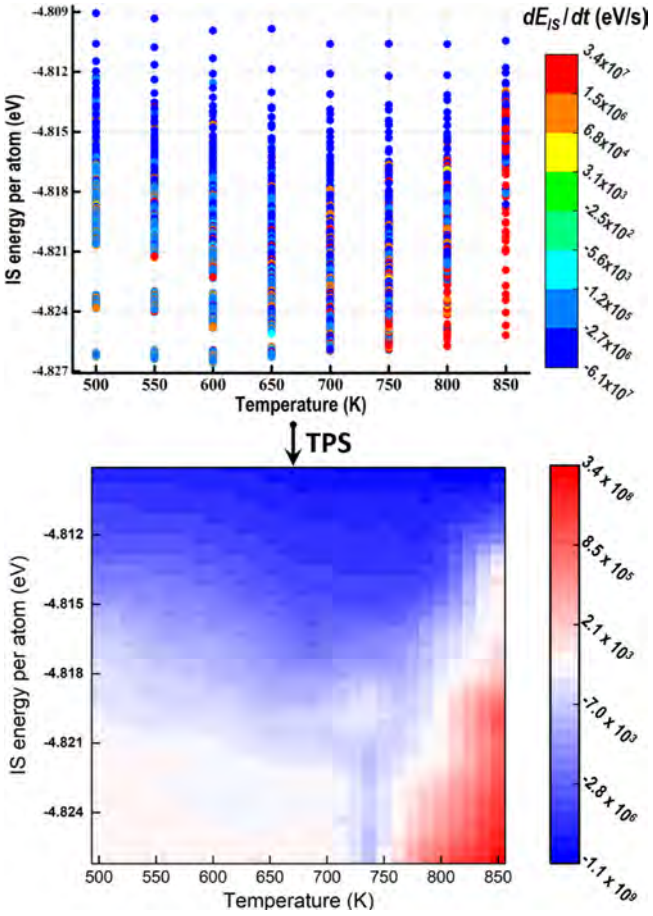

Fig. A1. (Up) Scattered data of E_{IS} variation rate at prescribed temperature and IS energy states. These discrete data are got from isothermal annealing curves of different samples in MD simulation by using the enhanced statistical method. (Down) A following TPS interpolation will convert these data points into a quasi-continuum pixel plot.

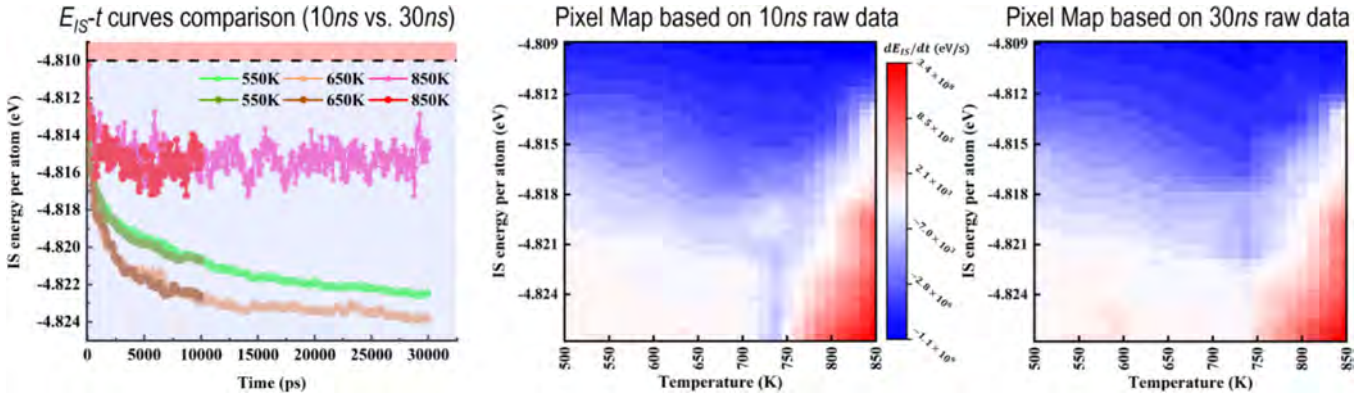

Fig. A2. There are no discernable changes to the non-monotonic ageing behaviors in the modeling with different length of simulation time.

starting from a given initial (E_{IS}, T) condition, the temperature is updated after each step of numerical integration. For example, assuming the numerical integration time step is Δt and the prescribed DSC scanning rate is α, then the temperature is updated as $T_{i+1} = T_i + \Delta t \cdot \alpha$. The temperature change will affect the value of $\langle E_A \rangle$ through Eq. (2), which will in turn change the energy variation rate in Eq. (1), and so on and so forth. The results in Fig. 4(c) are thus obtained.

References

[1] W.H. Wang, The elastic properties, elastic models and elastic perspectives of metallic glasses, Prog. Mater. Sci. 57 (3) (2012) 487–656.
[2] B.A. Sun, W.H. Wang, The fracture of bulk metallic glasses, Prog. Mater. Sci. 74 (2015) 211–307.
[3] C.A. Schuh, T.C. Hufnagel, U. Ramamurty, Mechanical behavior of amorphous alloys, Acta Mater. 55 (12) (2007) 4067–4109.
[4] M.Z. Ma, et al., Wear resistance of Zr-based bulk metallic glass applied in bearing rollers, Mater. Sci. Eng., A 386 (1) (2004) 326–330.
[5] S.J. Pang, T. Zhang, K. Asami, A. Inoue, Synthesis of Fe–Cr–Mo–C–B–P bulk metallic glasses with high corrosion resistance, Acta Mater. 50 (3) (2002) 489–497.
[6] M.D. Demetriou, et al., A damage-tolerant glass, Nat. Mater. 10 (2) (2011) 123–128.

[7] M. Zhao, K. Abe, S-i Yamaura, Y. Yamamoto, N. Asao, Fabrication of Pd–Ni–P metallic glass nanoparticles and their application as highly durable catalysts in methanol electro-oxidation, Chem. Mater. 26 (2) (2014) 1056–1061.
[8] P. Sharma, H. Kimura, A. Inoue, E. Arenholz, J.H. Guo, Temperature and thickness driven spin-reorientation transition in amorphous Co-Fe-Ta-B thin films, Phys. Rev. B 73 (5) (2006) 052401.
[9] W. Diyatmika, J.P. Chu, B.T. Kacha, C.-C. Yu, C.-M. Lee, Thin film metallic glasses in optoelectronic, magnetic, and electronic applications: a recent update, Curr. Opin. Solid State Mater. Sci. 19 (2) (2015) 95–106.
[10] B.W. An, et al., Stretchable, transparent electrodes as wearable heaters using nanotrough networks of metallic glasses with superior mechanical properties and thermal stability, Nano Lett. 16 (1) (2016) 471–478.
[11] S.V. Ketov, et al., Rejuvenation of metallic glasses by non-affine thermal strain, Nature 524 (2015) 200.
[12] M. Wakeda, J. Saida, J. Li, S. Ogata, Controlled rejuvenation of amorphous metals with thermal processing, Sci. Rep. 5 (2015) 10545.
[13] N. Miyazaki, M. Wakeda, Y.-J. Wang, S. Ogata, Prediction of pressure-promoted thermal rejuvenation in metallic glasses, Npj Comput. Mater. 2 (2016) 16013.
[14] B.A. Isner, D.J. Lacks, Generic rugged landscapes under strain and the possibility of rejuvenation in glasses, Phys. Rev. Lett. 96 (2) (2006) 025506.
[15] Y. Tong, W. Dmowski, H. Bei, Y. Yokoyama, T. Egami, Mechanical rejuvenation in bulk metallic glass induced by thermo-mechanical creep, Acta Mater. 148 (2018) 384–390.
[16] A. Gulzar, Z.G. Zhu, K. Shahzad, D.Q. Zhao, W.H. Wang, Flow units perspective on sensitivity and reliability of metallic glass properties, Intermetallics 69 (2016) 98–102.
[17] A. Slipenyuk, J. Eckert, Correlation between enthalpy change and free volume reduction during structural relaxation of Zr55Cu30Al10Ni5 metallic glass, Scr. Mater. 50 (1) (2004) 39–44.
[18] Y. Fan, T. Iwashita, T. Egami, Energy landscape-driven non-equilibrium evolution of inherent structure in disordered material, Nat. Commun. 8 (2017) 15417.
[19] F.H. Stillinger, A topographic view of supercooled liquids and glass formation, Science 267 (5206) (1995) 1935–1939.
[20] S. Sastry, P.G. Debenedetti, F.H. Stillinger, Signatures of distinct dynamical regimes in the energy landscape of a glass-forming liquid, Nature 393 (1998) 554.
[21] P.G. Debenedetti, F.H. Stillinger, Supercooled liquids and the glass transition, Nature 410 (2001) 259.
[22] D.J. Lacks, M.J. Osborne, Energy landscape picture of overaging and rejuvenation in a sheared glass, Phys. Rev. Lett. 93 (25) (2004) 255501.
[23] W. Kob, F. Sciortino, P. Tartaglia, Aging as dynamics in configuration space, Europhys. Lett. 49 (5) (2000) 590–596.
[24] A.L. Greer, J.A. Leake, Structural relaxation and crossover effect in a metallic glass, J. Non-Cryst. Solids 33 (2) (1979) 291–297.
[25] L. Boesch, A. Napolitano, P.B. Macedo, Spectrum of volume relaxation times in B2O3, J. Am. Ceram. Soc. 53 (3) (1970) 148–153.
[26] F. Shimizu, S. Ogata, J. Li, Yield point of metallic glass, Acta Mater. 54 (16) (2006) 4293–4298.
[27] H. Kallel, N. Mousseau, F. Schiettekatte. Evolution of the Potential-Energy Surface of Amorphous Silicon. (Translated from English), Physical Review Letters 105 (4) (2010) 045503 (in English).
[28] E. Cances, F. Legoll, M.C. Marinica, K. Minoukadeh, F. Willaime. Some improvements of the activation-relaxation technique method for finding transition pathways on potential energy surfaces. (Translated from English), Journal of Chemical Physics 130 (11) (2009) 114711 (in English).
[29] D. Rodney, C. Schuh, Distribution of thermally activated plastic events in a flowing glass, Phys. Rev. Lett. 102 (23) (2009) 235503.
[30] R. Srivastava, et al., Cooling rate evaluation for bulk amorphous alloys from eutectic microstructures in casting processes, Mater. Trans. 43 (7) (2002) 1670–1675.
[31] A. van den Beukel, J. Sietsma, The glass transition as a free volume related kinetic phenomenon, Acta Metall. Mater. 38 (3) (1990) 383–389.
[32] S.S. Tsao, F. Spaepen, Structural relaxation of a metallic glass near equilibrium, Acta Metall. 33 (5) (1985) 881–889.
[33] E.R. Homer, D. Rodney, C.A. Schuh, Kinetic Monte Carlo study of activated states and correlated shear-transformation-zone activity during the deformation of an amorphous metal, Phys. Rev. B 81 (6) (2010) 064204.
[34] Y.Q. Cheng, E. Ma, H.W. Sheng, Atomic level structure in multicomponent bulk metallic glass, Phys. Rev. Lett. 102 (24) (2009) 245501.
[35] P. Cao, M.P. Short, S. Yip, Potential energy landscape activations governing plastic flows in glass rheology, Proc. Natl. Acad. Sci. 116 (38) (2019) 18790.
[36] Z. Lu, W. Jiao, W.H. Wang, H.Y. Bai, Flow unit perspective on room temperature homogeneous plastic deformation in metallic glasses, Phys. Rev. Lett. 113 (4) (2014) 045501.
[37] C. Liu, P. Guan, Y. Fan, Correlating defects density in metallic glasses with the distribution of inherent structures in potential energy landscape, Acta Mater. 161 (2018) 295–301.
[38] J.S. Harmon, M.D. Demetriou, W.L. Johnson, K. Samwer, Anelastic to plastic transition in metallic glass-forming liquids, Phys. Rev. Lett. 99 (13) (2007) 135502.
[39] G.P. Johari, Localized molecular motions of β-relaxation and its energy landscape, J. Non-Cryst. Solids 307–310 (2002) 317–325.
[40] H.-B. Yu, W.-H. Wang, K. Samwer, The β relaxation in metallic glasses: an overview, Mater. Today 16 (5) (2013) 183–191.
[41] K. Samwer, H.B. Yu, H.Y. Bai, W.H. Wang, The β-relaxation in metallic glasses, Natl. Sci. Rev. 1 (3) (2014) 429–461.
[42] H.-B. Yu, R. Richert, K. Samwer, Structural rearrangements governing Johari-Goldstein relaxations in metallic glasses, Sci. Adv. 3 (11) (2017) e1701577.
[43] H.-B. Yu, et al., Fundamental link between β relaxation, excess wings, and cage-breaking in metallic glasses, J. Phys. Chem. Lett. 9 (19) (2018) 5877–5883.
[44] B. Xu, M.L. Falk, J.F. Li, L.T. Kong, Predicting shear transformation events in metallic glasses, Phys. Rev. Lett. 120 (12) (2018) 125503.
[45] B. Wang, et al., Nanometer-scale gradient atomic packing structure surrounding soft spots in metallic glasses, Npj Comput. Mater. 4 (1) (2018) 41.
[46] J. Ding, et al., Universal structural parameter to quantitatively predict metallic glass properties, Nat. Commun. 7 (2016) 13733.
[47] Y. Fan, T. Iwashita, T. Egami, Evolution of elastic heterogeneity during aging in metallic glasses, Phys. Rev. E 89 (06) (2014) 062313.
[48] Y. Fan, T. Iwashita, T. Egami, How thermally activated deformation starts in metallic glass, Nat. Commun. 5 (2014) 5083.
[49] Y. Fan, T. Iwashita, T. Egami, Crossover from localized to cascade relaxations in metallic glasses, Phys. Rev. Lett. 115 (4) (2015) 045501.
[50] J. Ding, S. Patinet, M.L. Falk, Y. Cheng, E. Ma, Soft spots and their structural signature in a metallic glass, Proc. Natl. Acad. Sci. 111 (39) (2014) 14052.
[51] A. Kushima, et al., Computing the viscosity of supercooled liquids, J. Chem. Phys. 130 (22) (2009) 224504.
[52] A. Widmer-Cooper, H. Perry, P. Harrowell, D.R. Reichman, Irreversible reorganization in a supercooled liquid originates from localized soft modes, Nat. Phys. 4 (2008) 711.
[53] P. Cao, M.P. Short, S. Yip, Understanding the mechanisms of amorphous creep through molecular simulation, Proc. Natl. Acad. Sci. 114 (52) (2017) 13631.
[54] P.M. Derlet, R. Maaß, Thermally-activated stress relaxation in a model amorphous solid and the formation of a system-spanning shear event, Acta Mater. 143 (2018) 205–213.
[55] S. Büchner, A. Heuer, Potential energy landscape of a model glass former: thermodynamics, anharmonicities, and finite size effects, Phys. Rev. E 60 (6) (1999) 6507–6518.
[56] G. Donato, S. Belongie, Approximate thin plate spline mappings, in: A. Heyden, G. Sparr, M. Nielsen, P. Johansen (Eds.), Computer Vision — ECCV 2002, Springer, Berlin Heidelberg, 2002, pp. 21–31.
[57] C. Deng, C.A. Schuh, Atomistic simulation of slow grain boundary motion, Phys. Rev. Lett. 106 (4) (2011) 045503.